3.1. Introduction

Organic conjugated polymers have become prominent semiconducting materials for those devices which are based on charge transport and charge separation properties. These devices include solar cells, organic field effect transistors, biosensors, and diodes which contain such type of semiconducting polymers as active material [Maria et al. (2017), Teran et al. (2016), Ivanović et al. (2016), Zhang et al. (2016), Han et al. (2016)]. It has been believed that, this semiconducting materials exhibit macroscopic charge transport properties through charge conduction combined from highly crystalline regions and poorly non-crystalline domains [Mollinger et al. (2015)]. Hence, charge transport phenomenon is highly anisotropic in nature [Kang et al. (2016)]. Therefore, in order to improve overall device performance, controlling the morphology through in-plane ordering (fibrous state) in such polymer is necessary. For instance, assembly in polymers should be in such a way that their crystallographic direction is along the active electrode to get improved charge conduction [Kleinhenz et al. (2016)]. The regioregular polymers having π- conjugated backbone (delivers structural rigidity) along with non-conjugated long alkyl side chains (imparts solubility) are regarded as excellent candidate to this context. It includes regioregular pure polymers (e.g. poly (3-n-alkylthiophene), where 'n' is alkyl chain with C-4 (butyl), C-6 (hexyl), C-8 (octyl), C-10 (decyl), C-12 (dodecyl); Poly (3,3‴-didodecylquarterthiophene), PQT-12; Poly[2, 5-bis (3-dodecylthiophen-2-yl)thieno[3,2-b]thiophene, pBTTT-C12; Poly[2, 5-bis (3-tetradecylthiophen-2-yl)thieno[3,2-b]thiophene, pBTTT-C14, and its derivatives (both grafted and block polymers e.g. poly (3-buytlthiophene)-b-poly (3-octylthiophene), poly(3-hexylthiophene)-graft-poly(2-vinylpyridine) and composites (e.g. PLA/P3HT) [Park et al. (2011), Kumar et al. (2014), Newbloom et al. (2014), Pandey et al. (2017), Singh et al. (2017), Risko et al. (2012), Xue

et al. (2015), Willot et al. (2015), Kim et al. (2016), Kim et al. (2014)]. Various strategies like vaporization induced self-assembly, ageing, poor solvent induced assembly, high temperature rubbing, electro-spinning, lithography, epitaxial crystallization etc. have been employed for the long-range ordering of such kind of polymer chains [Serrano et al. (2016), Gordon et al. (2016), Bounioux et al. (2016), Kleinhenz et al. (2016), Brinkmann et al. (2007), Biniek et al. (2013), Biniek et al. (2014)]. Among them, poor solvent induced ageing can be considered as an economic technique for long fiber formation. It has already been suggested that the aspect ratios of fiber depends on several factors like solution concentration, solvent choice, molecular weight and regioregularity of polymer used, cooling rate and some external interference such as ultrasonication, temperature, nature of substrate used etc. [Sun et al. (2011)]. The combinations of these factors affect the extent of solvent interaction with polymer. Particularly, in mixed solvent, good solvent is the majority solvent while poor solvent is minority solvent. Herein, good solvent expands the polymer chain, results more freedom to organize the chain; while poor solvent induces unfavourable interactions energy with polymer chains and create driving force for self-assembly of polymers [Kiriy et al. (2003), Scharsich et al. (2012), Traiphol et al. (2007)]. Among the poly (alkyl thiophene) families, pBTTT-C14 is considered as promising materials for organic transistors and photovoltaic cells due to high hole mobility (0.2–0.6 cm^2 V^{-1} S^{-1}) which is comparable to amorphous silicon [Beaujuge et al. (2011), McCulloch et al. (2006)]. Moreover, pBTTT-C14 exhibit crystalline order when subjected to a particular conditions like thermal annealing [Xue et al. (2015)], casting on liquid substrate, high temperature rubbing [Biniek et al. (2014)] etc. Literature survey reveals that there is a lack of information regarding self-assembly of pBTTT-C14 into fibrous state when exposed in solvent-mixture by ageing process. Therefore, in the present work, we tried out

to optimize the long-fiber formation in chloroform-toluene mixture at ambient temperature by ageing method followed by complete dissolution at elevated temperature. In this optimization experiments, on the basis of polarity index, chloroform is checked as good solvent while toluene is checked as poor solvent for pBTTT-C14. After that, as-prepared fibrous pBTTT-C14 dispersion is used for preparation of thin film having the thickness in nanometric range and further studied for its charge transport properties by sandwiching it between ITO and Al-metal, compared to the films formed from polymer dispersion in individual solvents.

3.2 Experimental

3.2.1 Materials

rr-pBTTT-C14 (M_w= 40K-80K, HOMO=5.1 eV, LUMO=3.1 eV) used for experimentation was purchased from Sigma-Aldrich, USA. Chloroform (analytical grade) and toluene (analytical grade) were purchased from Merck, India.

3.2.2 Optimization of pBTTT-C14 fibril formation

The pBTTT-C14 fibers were prepared by ageing of 0.005% w/v polymer dissolved in solution-mixture of different volume fraction for 17 minutes in a closed chamber equipped with temperature controller. Prior to this process, every polymer solutions were dissolved at 85°C and cooled to 25-27°C at 10 minute in corresponding solution-mixture. For the comparison purpose, same process is also adopted in chloroform and toluene solvent alone. The ageing time chosen here is optimized with the help of UV visible study as discussed latter. Solution-mixtures were prepared by mixing of chloroform (good solvent) and toluene (moderately poor solvents) in   1000:0, 950:50, 900:100, 850:150, 800:200 and 0:1000 ratio (v/v in μL) which is denoted subsequently as '0T' (0% Toluene), '50T' (5%

toluene), '100T' (10% toluene), '150T' (15% toluene), '200T' (20% toluene) and 'full T'(100 % toluene) respectively throughout the manuscript.

3.3. Results and discussion

One dimensional (1D) assembly of planer conjugated polymers into its fibrous state offer a possibility of directed charge transfer due to chain ordering along a feasible direction. The control of ordering of planer chain can be achieved by making interaction of polymers with solvent used. Particularly, in mixed-solvent, poor solvent derives the chain assembly while good solvent controls the morphology of fibers [Sun et al. (2011)]. Simultaneously, the evidence of chain assembly can be seen by changing its colour due to change in optical density of dissolved polymer upon addition of poor solvent followed by ageing and in the present case it is shown in Fig. 3.1(a) below. In this situation polymer tries to assemble either by face-on or edge-on manner as shown in Fig. 3.1 (b). In the present case, the growth of fiber is monitor by various tools as discussed one by one.
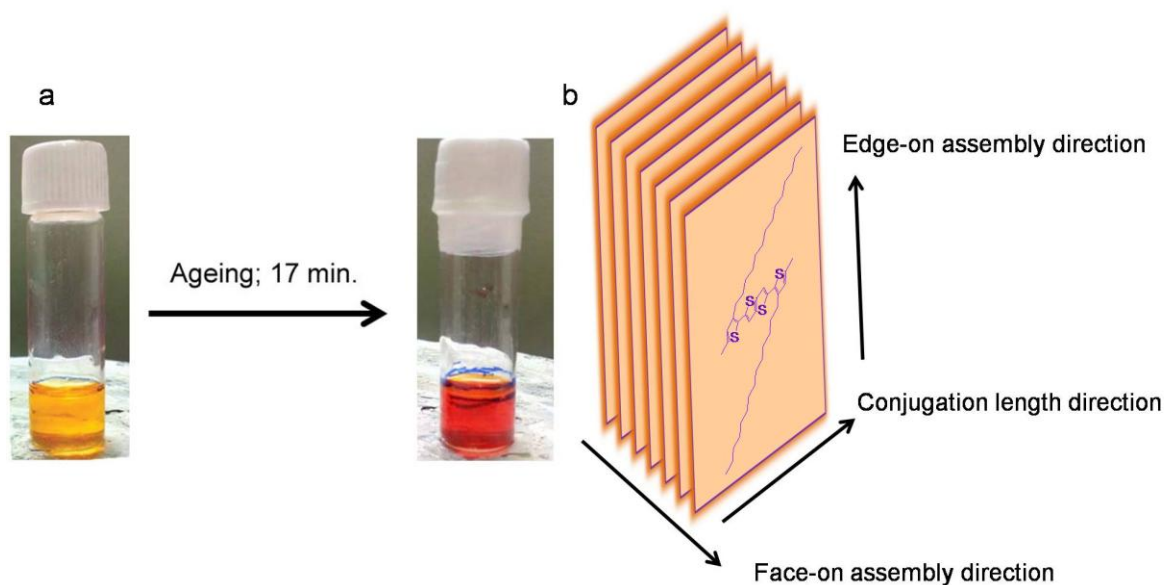

Fig. 3.1 (a) Photograph of Isolated (left) and aggregated pBTTT-C14 in 100T and (b) schematic representation of pBTTT-C14 assembly.

Optical analysis

The aggregations of pBTTT-C14 in pure chloroform (0T), pure toluene (full T) and different ratios of the solvent- mixtures (50T, 100T, 150T and 200T) were observed and compared with the help of UV visible spectroscopy ((EPOCH2C, Biotech Instrument Inc., USA).) as shown in Fig. 3.2 In general, pBTTT-C14 in its isolated state (complete dissolution upon heating in chloroform), gives one strong absorption peak at 470 nm due to $\pi \rightarrow \pi^*$ transition. In addition, it gives one another weak shoulder peak at 590 nm due to coupling of transition (π-$\pi*$) to the C=C (thiophene ring) similar to that of rr-PQT-12 and rr-P3HT upon ageing and followed by cooling at room temperature at a given condition [Kumar et al. (2014), Singh et al. (2017), Sun et al. (2011)]. The main peak intensity nominally decreases and shifted to higher wavelength with gradual increase in the shoulder peak upon ageing (shown in Fig.3.2 (I) a-f and *cf.* Fig. 3.2 (IV)a & Fig. 3.2 (V)a). This is due to self-assembly of polymers results change in optical density [Lohwasser et al. (2011)]. However, pBTTT-C14 in toluene solvent only, gives these two peaks (wavelength=465nm due to $\pi \rightarrow \pi^*$ transition and 590 nm due to coupling of this transition with C=C) even at its isolated state [10].Upon ageing followed by heating, it gives three distinct peaks (at 478 nm, 550nm and 590 nm), similar to rr-P3HT in toluene, indicating aggregation of polymer. The intensity of 465 nm peak gradually decreases with the slight shift to higher wavelength (from 465 to 478 nm) (shown in Fig. 3.2 (II)a-f and *cf.* Fig. 3.2 (IV)f & Fig. 3.2(V)f) [10]. On comparing these two extreme cases, we observed that the aggregation phenomenon of similar concentrations pBTTT-C14 is slower in chloroform than that of toluene at similar conditions. This is due to difference in polarity index (3.4-4.4 *vs.* 2.4) of solvents results different extent of interactions with polymer. That is why we tried to control the aggregation by similar conditions in presence of four different v/v ratios

of solvents-mixture. Thus, the corresponding UV visible spectra of polymer aggregation in four different solvent-mixtures are shown in Fig. 3.2 (III). In this case, we observed that polymer gives one strong peak at 476 nm which is shifted to 486 nm upon increase the amount of toluene. Apart from this, polymer gives two another weal shoulder peaks at 445nm and 590 nm respectively like in the case of toluene (shown in Fig. 3.2 (III) and *cf.* Fig. 3.2 (IV) b-e & Fig. 3.2 (V) b-e). On comparing these results with AFM analysis (as discussed latter), we concluded that the polymer aggregation performed in 100T resulted regular fiber with high aspect ratio in a large area. Therefore, the ageing time for polymer aggregation is optimized using this ratio of solvent-mixture (shown in Fig. 3.2 (VI)). In this case, polymer gives one strong peak at 477 nm along two weak shoulder peaks at 550 and 590 nm respectively like in full T. The polymer is aged for 10 h and aggregation behaviour is studied with interval of 60s corresponding to absorption peak at 590 nm (shown in Fig. 3.3(I)). We observed that the peak intensity gradually increases from zero to 17 min by 0.288 while it is only 0.001 after 17 to 9h. It means that 17 minute is optimal time for aggregation in solvent-mixture. The aggregation of pBTTT-C14 into fibrous form and its aspect ratio were further analyzed by AFM.

The confirmation of fiber formation was further exemplified by photoluminescence emission (PL) spectrophotometer (Perkin Elmer, LS-50B, USA), excited at 470nm for similar concentrations of pBTTT-C14 dispersion prepared in 100T (shown in Fig. 3.3(II)). The marginal decrement in emission intensity is seen in case of aggregated pBTTT-C14, which is due to dense packing and molecular orientation effectively along face-on direction similar to PQT-12 [Singh et al. (2017)]. This phenomenon was additionally justified by XRD, as explained later.
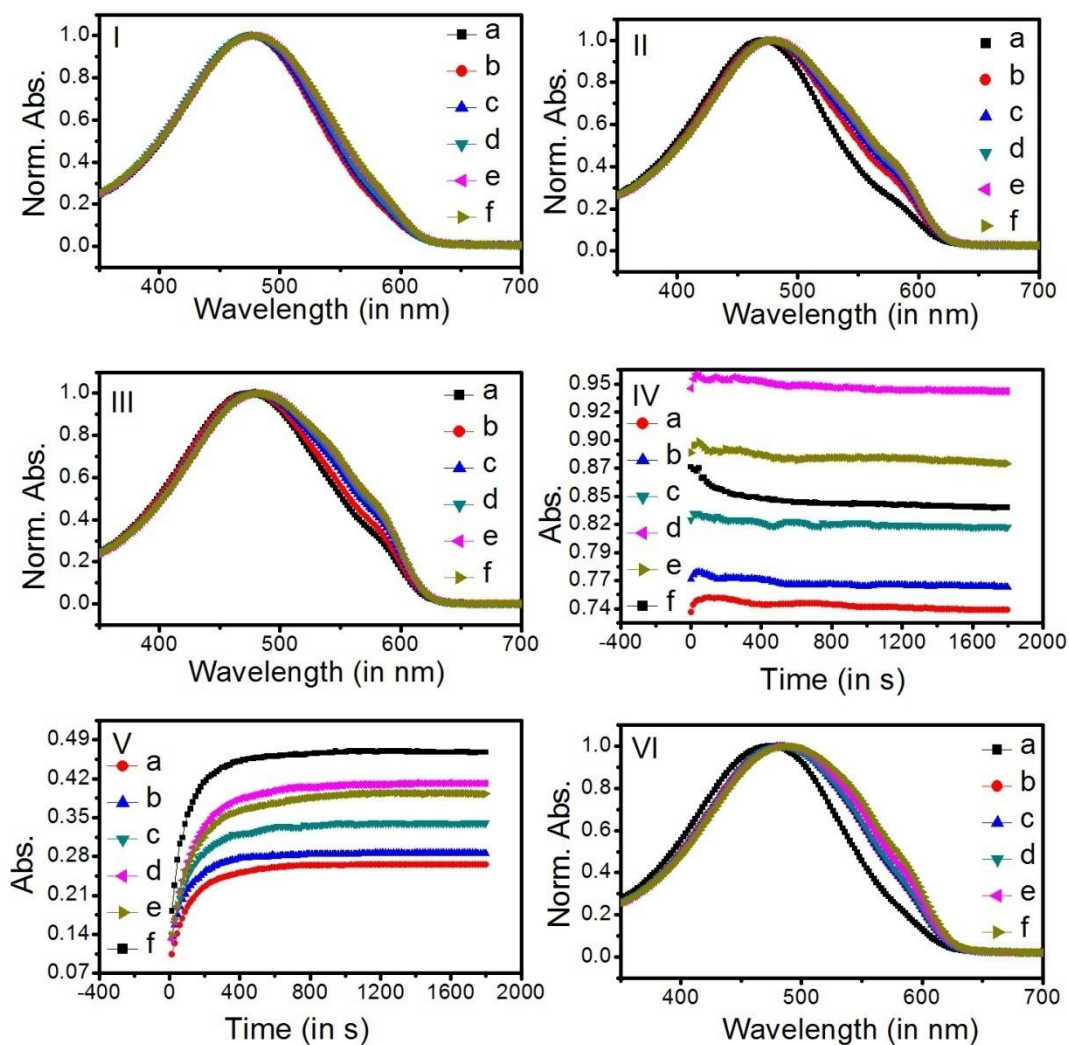
Fig.3.2 UV visible spectroscopy of pBTTT-C14 in 0T (I), full T (II) after successive time interval of 60s, UV visible spectroscopy of pBTTT-C14 in 0T (a), 50T (b), 100T (c), 150T (d), 200T (e) & full T (f)(III), absorbance kinetics of pBTTT-C14 in 0T (a), 50T (b), 100T (c), 150T (d), 200T (e) & full T (f) at wavelength= 470nm (IV) & 590 nm (V) and UV visible of pBTTT-C14 in 100T after successive time interval of 60 s (a-f) (VI).

In order to explain the molecular packing and nature of disorder due to polymer aggregations from their isolated state, Frank–Condon principle is anticipated to be a worthy methodology [Spano et al. (2010), Spano et al. (2005), Danesh et al. (2012)]. In general, the absorbance ratio, A' ($=A_{0-0}/A_{0-1}$) is considered for extent of aggregation and is related

to the aggregates' free exciton bandwidth (*W*) and the energy of the main intramolecular

vibration (*E_p*) coupled to the electronic transition by using equation (1) (supposing a
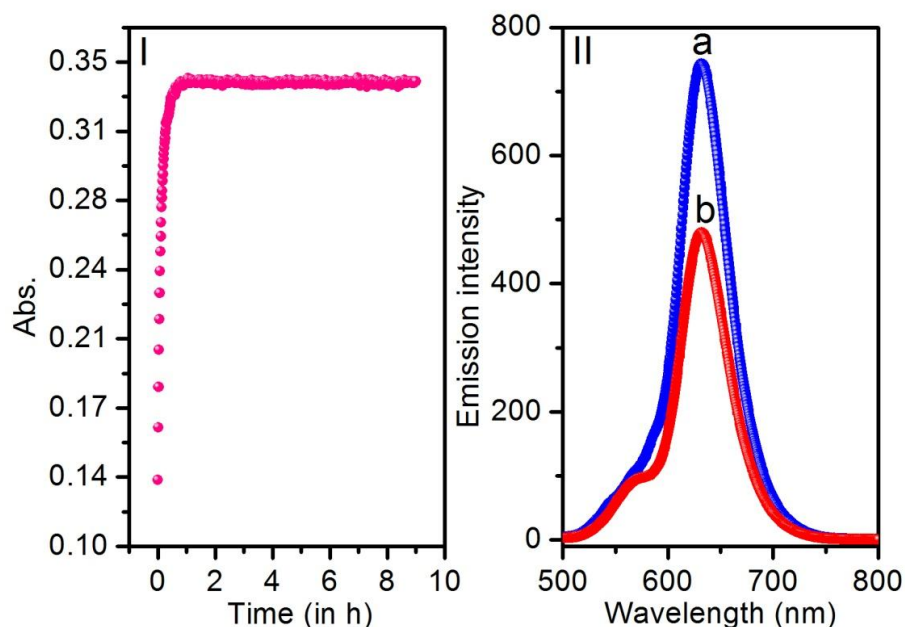
Huang–Rhys factor =1) [Spano et al. (2005)].

Fig. 3.3 (I) Absorption kinetics for 9 h at 590 nm and (II) photoluminescence spectra (PL) of (a) isolated & (b) aggregated pBTTT-C14 in100T.

 Since, the absorption spectra of aggregated pBTTT-C14 consists of mainly two parts—a

low energy part explains weakly interacting π-system (H-aggregates) and a high energy

part results due to more disordered chains like other polymers (rr-P3HT or rr-PQT-12)

[Wang et al. (2013)]. Therefore, various possible electronic transitions are well resolved by

Gaussian fitting [as shown in Fig. 3.4].

$$\frac{A_{0-0}}{A_{0-1}} \sim \left[\frac{1 - \frac{0.24W}{E_p}}{1 + \frac{0.073W}{E_p}} \right]^2 \qquad (1)$$

W is estimated using *A'* above equation by assuming the C=C symmetric stretching at 0.18 eV dominates the coupling to electronic transition [Louarn et al. (1996)]. A decrease of *W* [or increase of *A'* as shown in Fig. 3.4] with increase in concentration of toluene (except full T) is observed which is consistent with an increase of conjugation length, reflecting fiber-like conformation [Barford et al. (2007)]. In case of full T, the value of *A'* is suppressed suddenly due to dominance of three shoulder peaks over the main absorption peak similar to rr-P3HT in toluene [Kumar et al. (2014)].
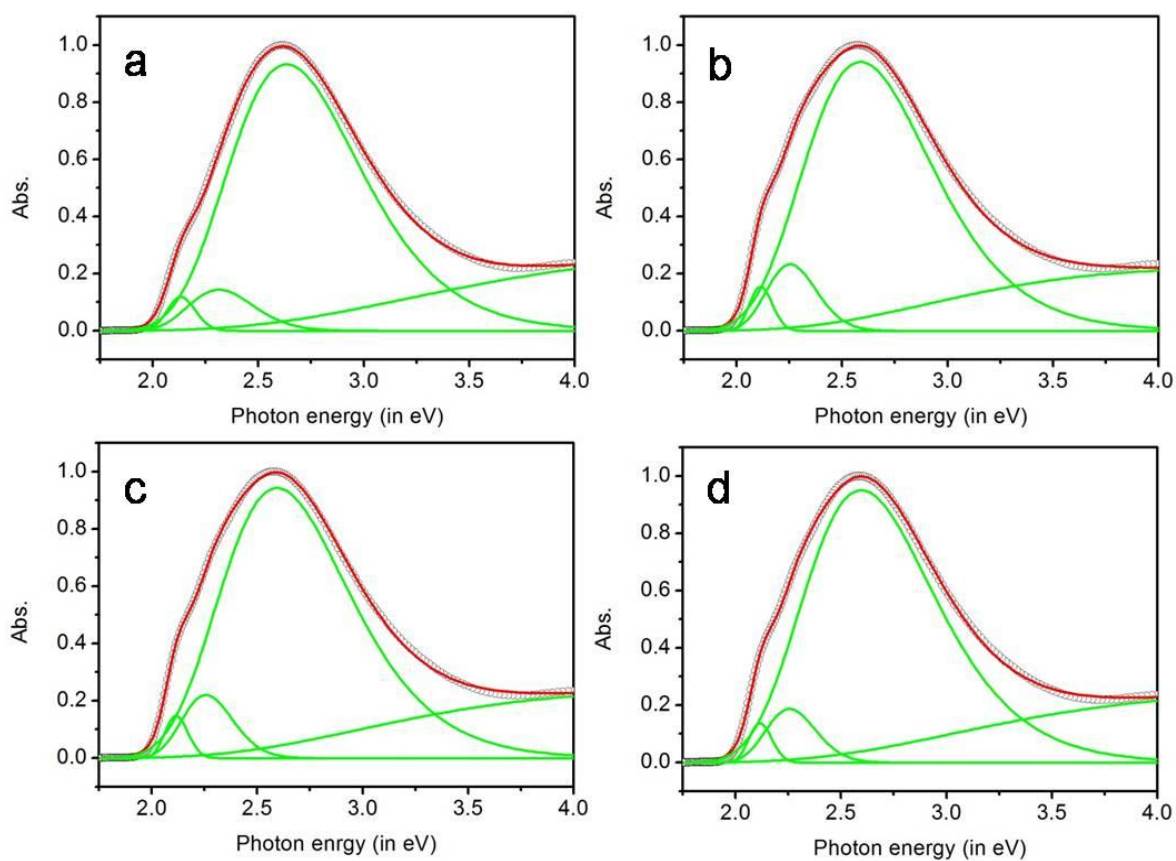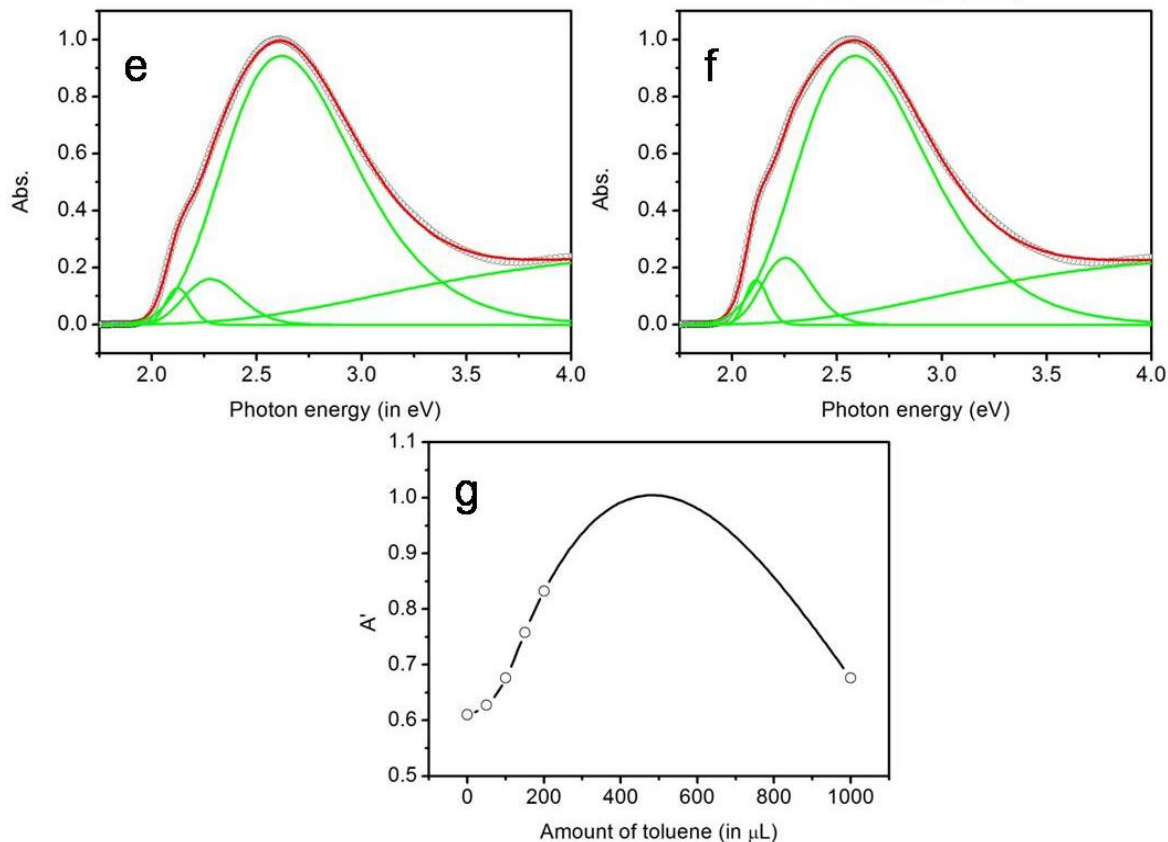
Fig. 3.4 Gaussian fitting UV visible plots of pBTTT-C14 dispersed in 0T (a), 50T (b), 100T (c), 150T (d), 200T, full T (f) and plot of *A'* (*=A_{0-0}/A_{0-1}*) *vs.* amount of toluene addition (g).

XRD analysis

The molecular packing analysis of pBTTT-C14 was further exemplified by XRD (Rigaku, Smart Lab, Japan) and shown in Fig. 3.5. The diffraction peaks at 3.9° and 7.8° are the consequence of d-spacing (lamellar structure) corresponding to (100) and (200) planes respectively towards face-on direction [Shi et al. (2014)]. However, in case of aggregated pBTTT-C14, these peaks shifted towards higher 2θ values (i.e. from 3.9° to 4.2° for (100) plane and from 7.8° to 8.4° for (200) plane) along with high intensity of (100) plane with respect to its isolated analogue (*cf.* Fig. 3.5 (a) and Fig. 3.5 (b)). This behaviour might be due to decrease in d-spacing, results from face-on orientation [Singh et al. (2017)].
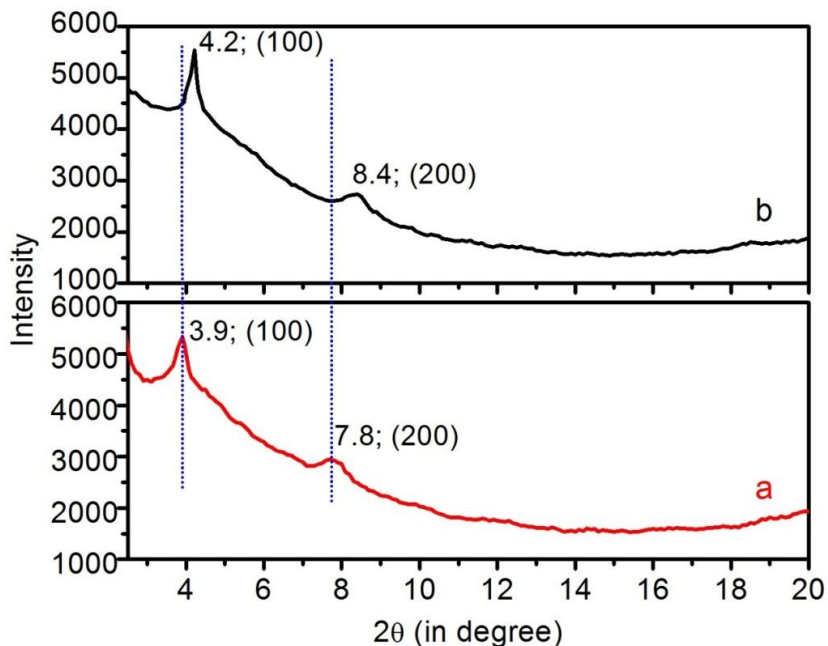
Fig. 3.5 XRD of (a) isolated & (b) aggregated pBTTT-C14 thin film in100T.

AFM analysis

In general interpretation, the fibril morphology is the signature of ordering in planer chains (as discussed in UV–visible analysis also) through π-stacking with the backbone axis perpendicular to the chain stacking direction as commonly observed in regioregular polymers with long alkyl side chains like rr-P3HT, rr-PQT-12 etc. [Singh et al. (2017), Lim et al. (2010), Liu et al. (2011)]. The substantial differences in morphology of pBTTT-C14 in all concentration of solvent-mixture were analysed using AFM (AFM, ND-MDT, NTEGRA Prima, Russia) by tapping imaging mode on spin casted film over ITO substrate as shown in Fig.3.6. The AFM images show fiber-like aggregation upon ageing of pBTTT-C14 in different solvents and its mixture at similar conditions from the isolated state (complete dissolution at 85ºC) (*cf.* Fig. 3.6(a-f) and Fig. 3.6(a'–f')). The darker area and ghter area of images represent depression and elevation in film respectively. It is clear from

these images, except the case of full T, there is no possibility of aggregation in pBTTT-C14. It means that polymers exist in disentangled form at its isolated state (*cf.* Fig. 3.6(a-e) and Fig. 3.6(f)). While upon ageing for 17 minute followed by complete dissolution at 85°C, the aggregation in polymer along most favourable side (face-on) occurs. The aggregation progress is lowest in case of chloroform (good solvent) and it is gradually increases (fiber content per unit volume) upon addition of toluene (poor solvent). However, fiber content slightly decreases upon addition of more toluene. It may be due to fast aggregation of chains into irregular manner (with little percentage of fibers). In case of toluene, the aggregation process is going to start just after cooling to 30°C from 85°C (Fig. 3.6(f)). It is no doubt that polymer is giving fibrous assembly in toluene only. But these aggregations process are too fast so that homogeneous fiber is not possible in a given area using proposed concentration of polymer (as shown in inset of Fig. 3.6(f')). In conclusion, we observed that growth of fibrous assembly is better in case of 100T than other counterparts. It means that choice of pBTTT-C14 in 100T is optimal for regular fiber formation under the given conditions.

The homogeneity in pBTTT-C14 fibers on large scale area (20x20 micron) were further analysed by AFM (topography and phase signal form) and TEM (shown in Fig. (3.7)). These fibers are semi-crystalline in nature with high aspect ratio (average diameter = 11nm and length = few microns) as evident by height profile and TEM analysis (*cf.* Fig. 3.7(c) and Fig. 3.7(e)).
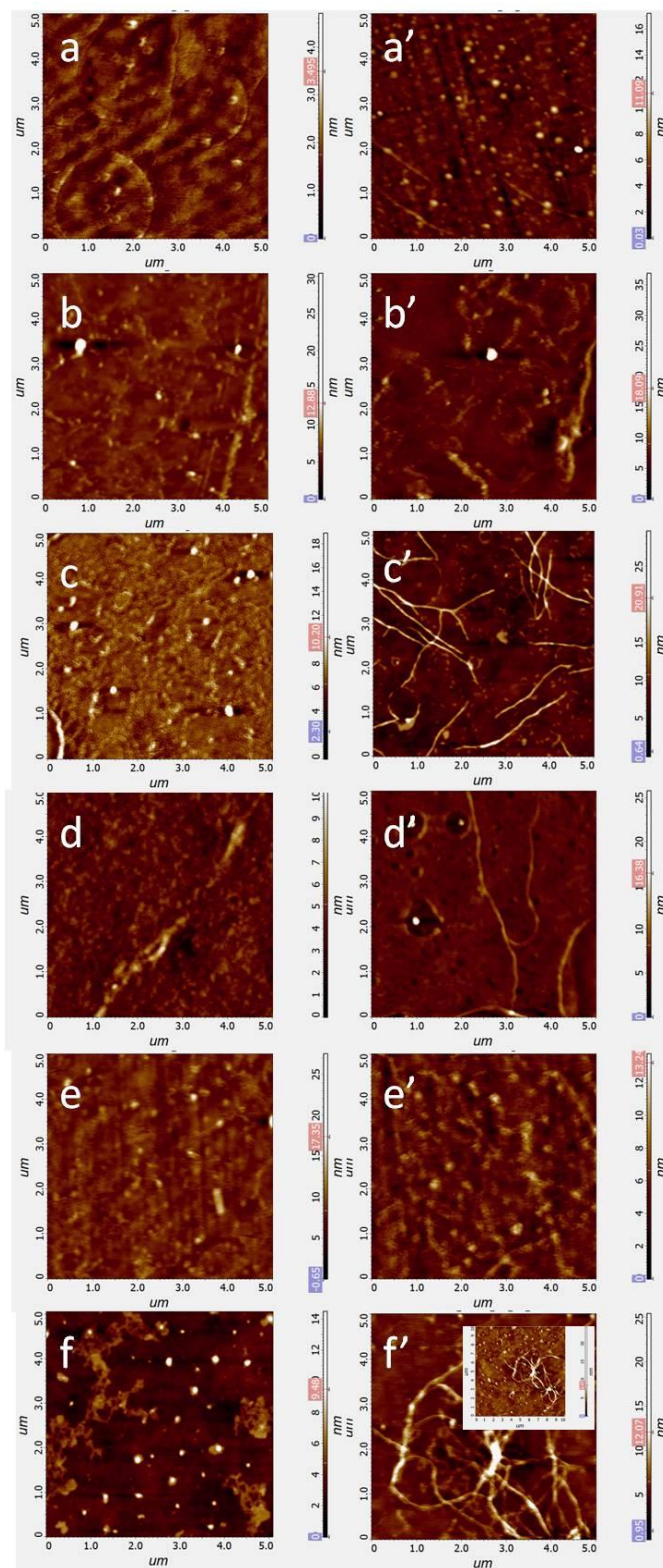
Fig. 3.6. AFM images of isolated (a-f) and aggregated (a'-f') pBTTT-C14 films prepared in 0T, 50T, 100T, 150T, 200T & full T. Inset of Fig. 3.6 (f') shows AFM of pBTTT-C14 film prepared in full T on large area.
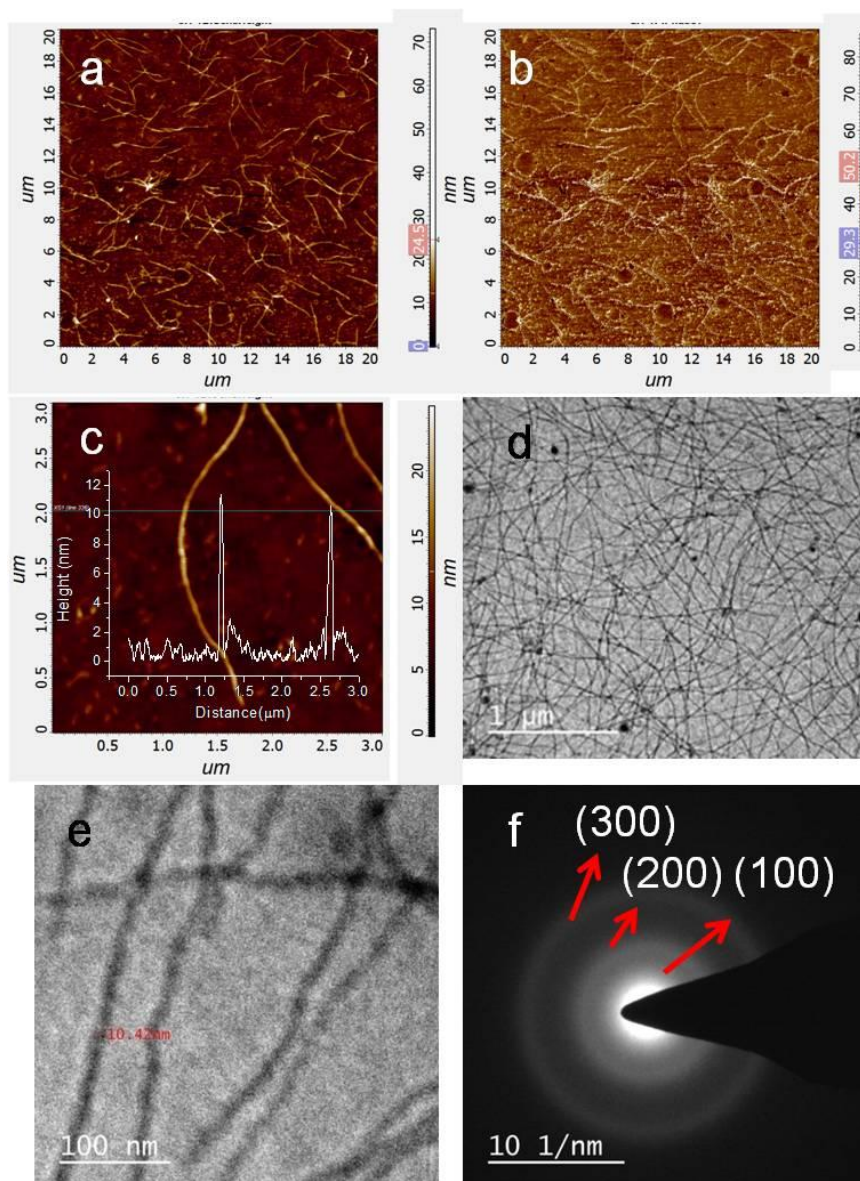
Fig. 3.7. Large area AFM and corresponding phase image (a & b), magnified AFM image with height profile (c), large area TEM image (d), HRTEM image (e) and SAED pattern of pBTTT-C14 fiber prepared in 100T.

The surface potential imaging of fibrous pBTTT-C14, coated over glass substrate was further verified by Kelvin probe force microscopy, KPFM together with AFM (both topographic and phase mode) using Si coated Pt-tip (work function= 5.69 eV) biased at 3.0 V which is shown in Fig.3.8. In this technique, two fibers together along with neat surfaces were targeted for the study of variation in surface potentials. From KPFM image, it is clear

that the surface potential is increased by approximately 6.0 V (left fiber) and 4.5 V (right fiber) with respect to neat surface (*cf.* Fig. 3.8(c) and Fig. 3.8(d)). This is due to involvement of trap filled charges within the π-stack regions. This evidence can also be seen in case of junction property study (as discussed latter).
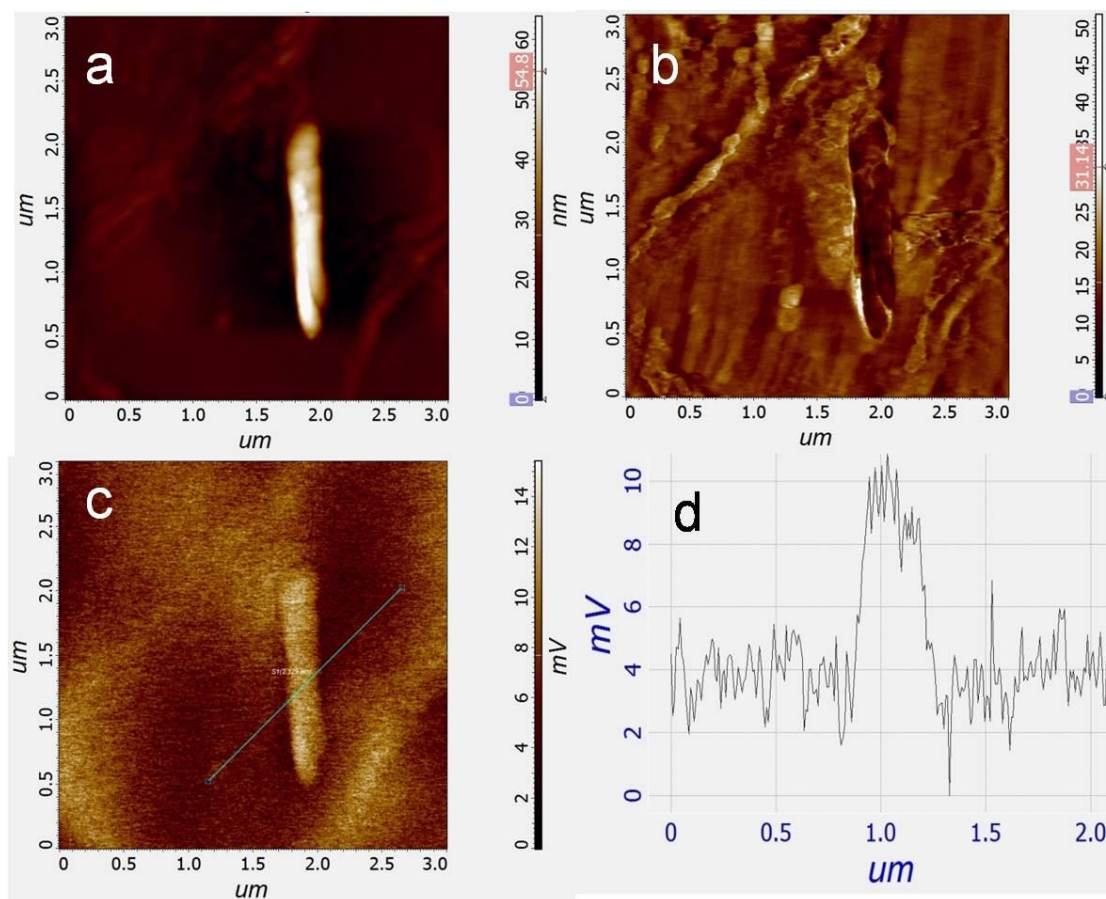

Fig. 3.8. AFM in topographic (a), phase (b) and KPFM (c) of fibrous pBTTT-C14 prepared in 100T.

Fabrication of device and study of charge transport properties:

In order to get the proper intimacies of two highly conducting material (ITO and Al-metal) between PBTT-C14, following procedures were adopted. First of all commercially available ITO was cleaned with chloroform followed by toluene. After that 20 µL fibrous

pBTTT-C14 dispersion (100T) was spin casted (rpm= 2500, 30s) over ITO. Now, dots of Al-metal (thickness= 120 nm) were thermally grown over polymer coated on ITO using thermal evaporation unit (124AD, Hind High Vac, Bangalore, India).

Similar procedure was adopted for isolated polymer analogue in order to make comparative study.

In general, it has been reported that, in case of polyalkylthiophenes-metal (with low work function than polymer) contacts, the nature of J-V behaviour is closely (but not exactly) comparable to Schottky type nature observed in conventional semiconductors. In which, it has suggested that, a thermally activated bulk conductivity (through hopping process in polymer) in series with a tunnelling process (through barrier) are responsible for these type of electron transition behaviour and, is more closely to a thermionic emission process in series with the bulk conductivity observed in case of conventional semiconductors [Tomozawa et al. (1989), Brédas et al. (2012)]. In view of these facts, the junction behaviours parameters have been extended using thermionic emission theory for several devices fabricated using metal-polymer contacts since long time and also extended in present case of study [Singh et al. (2010), Sze (1981)]. J-V and log J-V characteristics of as-fabricated junctions (as shown in inset of Fig. 3.9) of isolated and aggregated pBTTT-C14 film prepared in 100T between ITO (bottom electrode) and Al (top electrode) is shown in the Fig. 3.9. Since, it has been reported that the charge transport characteristics between polymer and ITO is Ohmic in nature [Nakanishi et al. (1999)]. Therefore, we are observing here, the response of applied potentials between Al and polymer only. It is clear that the forward current density (at 1.0 V) of aggregated pBTTT-C14 is ~ 6.5 times higher as compared to that of isolated pBTTT-C14 (0.91 A/cm^2 *vs.* 0.14 A/cm^2) (*cf.* Fig. 3.9(a) and

Fig. 3.9(b)). This is due to the involvement of charge conduction path across the fiber

assembly that possess entrapped charge [Nikitenko et al. (2003)]. Similarly, aggregated

pBTTT-C14 exhibits relatively lower leakage current under reversed biased condition in

comparison to its isolated analogue. Several parameters like ideality factor (η), barrier

height (Φ_B), saturation current density (J_o), and rectification ratio (RR) have been evaluated

(assuming the current is due to thermionic emission).The relation between the applied bias

voltage (forward bias) and current density can be expressed as [Rhoderick and William

(1988)]-

$$J = J_0 exp\left(\frac{qV}{\eta kT}\right)\left[1 - exp\left(\frac{-qV}{kT}\right)\right] \tag{2}$$

For V>3kT/q eq. (1) will be-
$$J = \frac{I}{A} = J_0 exp\left(\frac{qV}{\eta kT}\right) \tag{3}$$

Where
$$J_0 = A^*T^2 exp\left(\frac{-q\Phi_B}{kT}\right) \tag{4}$$

From eq. (2)
$$\eta = \frac{q}{kT}\left(\frac{\delta V}{\delta(ln\,J)}\right) \tag{5}$$

In eq. (3), J denotes current density(in A cm^{-2}), A- effective diode area (equals to 7.85×10^{-3}

cm^2 in our case) q- electronic charge, V- bias voltage, η- ideality factor (can be extracted

from slope of the linear region of the lnJ-V plot) , k- Boltzmann constant, T- temperature

(in K) and J_0 denotes the saturation current density (can be obtained by extrapolating the

linear region of lnJ line to zero bias voltage in lnJ-V plot). In eq. (4), A^*- effective

Richardson constant (equals to 120 A cm^{-2}K^{-2}) and Φ_B is the zero-bias barrier height.

All the parameters are calculated and tabulated in the Table 3.1. The junction prepared using aggregated pBTTT-C14 film exhibit low turn-on voltage with high RR ratio and mobility even on nearly comparable 'Φ_B' with respect to that of its isolated analogue. This is due to involvement of trapped charged between π-stacked regions upon biased condition [Singh et al. (2017)]. Similarly, due to trap-assisted tunneling, the carrier leakage and inhomogeneous barrier responsible for deviation of 'η' from its ideality [49]. The lowering of η-value is due to filling of traps in case of aggregated pBTTT-C14.

In order to explain the charge conduction mechanism, the J-V curves are re-plotted in a double logarithmic J-V form (shown in **Fig.3.10**). It is well known that, conducting polymer exhibit exceptional charge transport mechanism which is collectively associated with delocalization and localization of charge carriers in intramolecular and intermolecular charge interaction respectively. From the J-V characteristics, based upon the value of slope 'τ' (in J α V$^{\tau}$), the three basic regions *viz.* the Ohmic current (Ohm), trap-limited/trap-filling space charge limited current (TLSCLC), and trap-free space charge limited current (TFSCLC) regions respectively are nominated in the case of polymers like rr-P3HT, rr-PQT-12 [Mollinger et al (2015), Sun et al (2011), Spano (2010), Rose et al. (1955)]. The drift current flows by sweeping of thermally generated carriers under applied potential in Ohmic region (slope ~1) at low bias. Similarly, on increasing the bias voltage, the charge carriers are being gradually injected from electrode into polymer in TLSCLC region (1≤ slope <2), but the polymer is unable to transport them with equivalent rate due to trapping of some charge carriers into the polymer, this might be because of presence of shallow traps in TLSCLC [Chiguvare et al. (2012)]. Further, the process of filling of low energy traps are initiated as the potential increases which ultimately leads to accumulation of the

excess charge carriers in the polymer near to injecting electrode (space charge region). This process ends until all low energy trap levels are filled up [Chiguvare et al. (2012)]. Hence, the total current flowing in this region is the addition of the current of Ohm region and that of TFSCLC region (i.e. $J_{TLSCLC} = J_{Ohm} + J_{TFSCLC}$; where $J_{Ohm} = qn\mu {V}/{d}$). The trapping of carrier in this region is mainly due to structural orientation or some defects, which allows localization of charges. For example, trapping of carrier is possible within the π-stacks of individual polymers and are short lived [Schmechel et al. (2004)]. When applied voltage exceeds the average energy associated with trap density, polymer behaves like TFSCLC (τ=2) as seen in case of fibrous pBTTT-C14 (see Fig. 3.10). Here, in case of aggregated pBTTT-C14, (a) Ohmic (τ ~1), (b) TLSCLC (τ ~1.41) and (c) TFSCLC (τ ~2.19) regimes are seen. But, in the case of isolated pBTTT-C14, the intermediate regime (TLSCLC) is not seen (or may merged with ohm regime'd'), due to lack of localization of charges, trapped within π-stacks. Particularly, in TFSCLC region (regime 'c'), the filling of trap distribution occur exponentially in case of fibrous pBTTT-C14 and is of maximum density near the band edge compared to isolated pBTTT-C14 (slope of regime 'c' (2.19) is higher than that of regime 'e' (1.91)). Further it has been assumed that, almost all trap centres are occupied by injected charge carriers on/after the intersection of 'b' and 'c' regimes [Nikitenko et al. (2003), Chiguvare et al. (2004), Pasveer et al. (2005)]. That is why, anomalous increment in current density is observed under short applied voltage range in case of fibrous pBTTT-C14 [Singh et al. (2017)].

The relative charge carrier mobility, *μ* of pBTTT-C14 (both aggregated and non-aggregated) is calculated by Mott-Gurney's equation (equation 7) by assuming almost

same thickness (~100nm, calculated by AFM and shown in Fig. 3.11) of film and completely filled traps [Pasveer et al. (2005)].

$$J_{\text{TFSCLC}} = \frac{9}{8}\varepsilon\mu\frac{V^2}{d^3} \qquad (7)$$

Here **J-** current density (in A/cm^2), **μ-** mobility (in cm^2/Vs), **d-** thickness (in m) of film and **V-** voltage (in V) applied across the film, **ε-** dielectric permittivity of film and it is taken as1.55 [Porrazzo et al. (2015)].
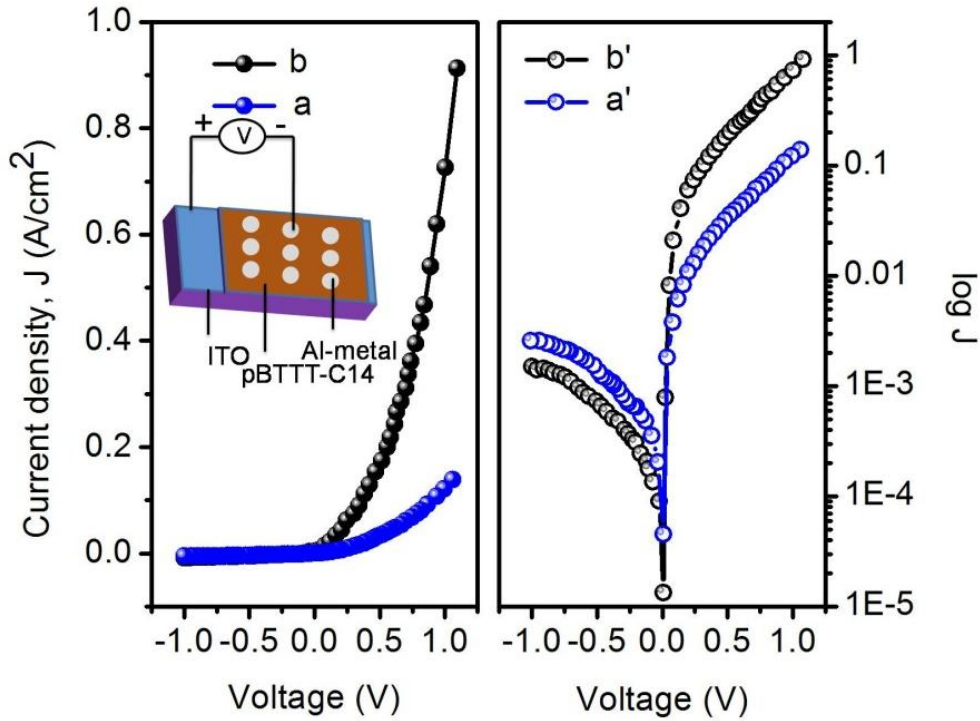

Fig.3.9. *J-V* and *logJ-V* characteristics of isolated (a & a') and aggregated (b & b') pBTTT-C14 prepared in 100T based devices respectively. Inset represents device schematic.

The mobility is calculated into the trap-free SCLC (TFSCLC) region (slope~2; as per eq. 7) in the double logarithmic (J-V) plots shown in Fig. 3.10. From here, the calculated intrinsic carrier mobility in pBTTT-C14 fiber is found to be 9 times higher than that of its isolated analogue. This ultimately results from the aggregation of chain along π-π direction which

favours inter chain free charge conduction by hopping process similar to that of rr-P3HT or

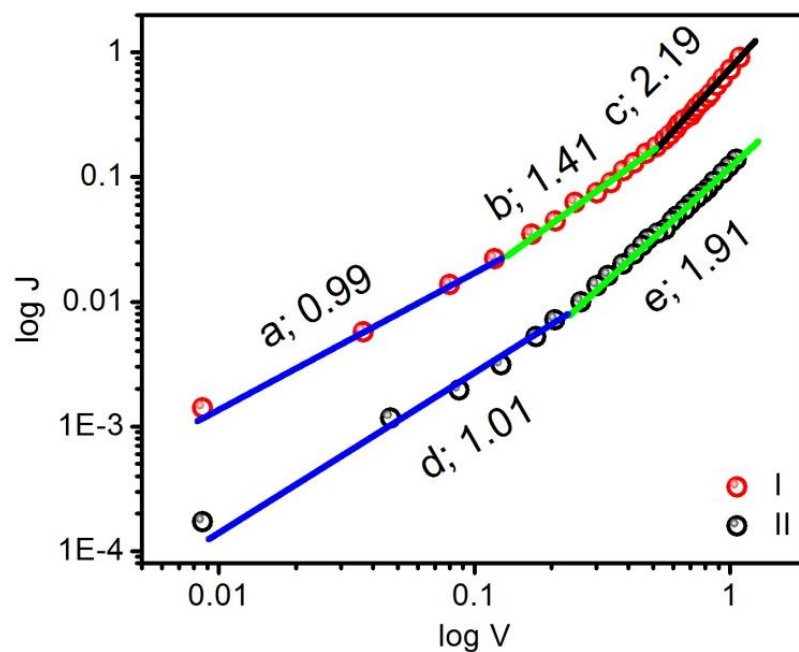rr-PQT-12 [Singh et al. (2017), Nikitenko et al. (2003), Salleo (2007)].

Fig.3.10. Double logarithmic (J-V) plot of aggregated (I) and isolated (II) pBTTT-C14 prepared in 100T based devices respectively.
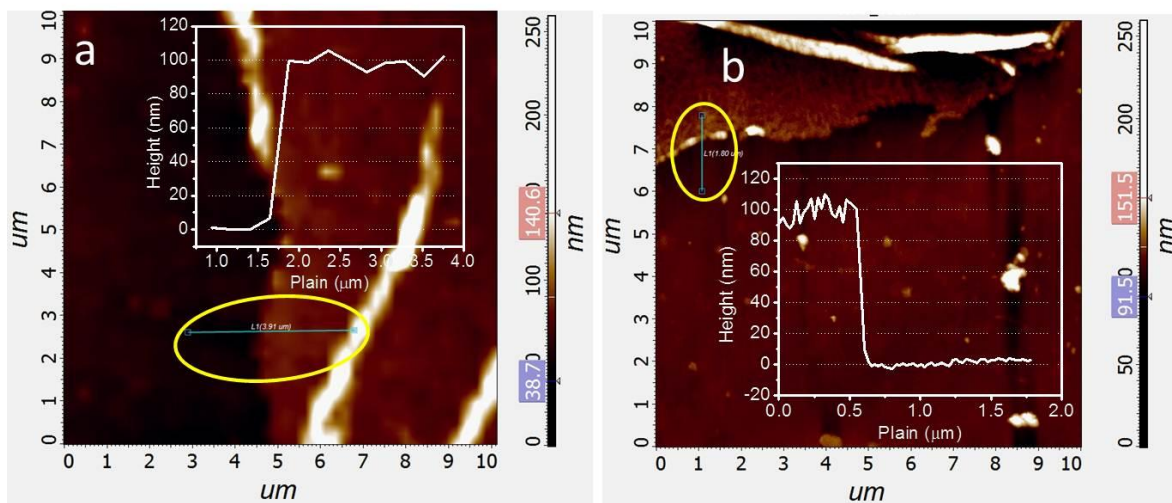

Fig. 3.11. Film thickness measurement by AFM for (a) isolated and (b) aggregated pBTTT-C14 prepared in 100T.

Table 3.1. Electrical device parameters

Parameters	Aggregated pBTTT-C14	Isolated pBTTT-C14
Barrier Height $\Phi_B(eV)$	0.698±0.011	0.671±0.015
Turn-on Voltage T_{ON} (V)	0.415	0.471
Saturation Current Density J_0 (A/cm^2)	$(1.741±0.121)×10^{-5}$	$(7.593±0.101)×10^{-5}$
Ideality Factor (η)	2.32	3.29
Rectification Ratio (-1.0 to 1.0 V)	707	66
Mobility (cm^2/Vs)	$6.99×10^{-3}$	$7.67×10^{-4}$

3.4. Conclusion

The p-BTTT-C14 fiber preparation is optimized successfully in solvent-mixture due to solvophobic interaction of polymer chains and solvent molecules. The fiber with high aspect ratio (diameter=11nm and length= few microns) can be prepared successfully by just ageing the polymer for 17 minutes followed by heating at 85ºC in solvent mixture of chloroform (good solvent) and toluene (poor solvent) in 9:1 ratio v/v. The experimental observations exemplify that addition of poor solvent plays decisive role for the aggregation of pBTTT-C14 into fiber form. The fiber growth predominantly occurs along π-π stacking direction similar to rr-PQT-12. The device based on film of as-aged dispersion, exhibits better charge transport properties (~6.5 times higher forward current density and ~9 times higher mobility) with improved ideality factor, low turn-on voltage and high rectification ratio than that of its isolated analogue. This is due to inclusion of favorable charge transport path that possess trap filled charge carriers. We hope that our optimization strategy will be creating future opportunity for other devices or use of material in other applications.